A scaled boundary node method applied to two-dimensional crack problems*

Chen Shen-Shen(陈莘莘)[a)†], Li Qing-Hua(李庆华)[a)], and Liu Ying-Hua(刘应华)[b)]

[a)] *College of Civil Engineering, Hunan University of Technology, Zhuzhou* 412007, *China*

[b)] *Department of Engineering Mechanics, School of Aerospace, Tsinghua University, Beijing* 100084, *China*

(Received 26 April 2012; revised manuscript received 20 June 2012)

A boundary-type meshless method called the scaled boundary node method (SBNM) is developed to directly evaluate mixed mode stress intensity factors (SIFs) without extra post-processing. The SBNM combines the scaled boundary equations with the moving Kriging (MK) interpolation to retain the dimensionality advantage of the former and the meshless attribute of the latter. As a result, the SBNM requires only a set of scattered nodes on the boundary, and the displacement field is approximated by using the MK interpolation technique, which possesses the δ function property. This makes the developed method efficient and straightforward in imposing the essential boundary conditions, and no special treatment techniques are required. Besides, the SBNM works by weakening the governing differential equations in the circumferential direction and then solving the weakened equations analytically in the radial direction. Therefore, the SBNM permits an accurate representation of the singularities in the radial direction when the scaling center is located at the crack tip. Numerical examples using the SBNM for computing the SIFs are presented. Good agreements with available results in the literature are obtained.

Keywords: meshless method, scaled boundary node method, moving Kriging interpolation, stress intensity factor

PACS: 02.60.Cb, 02.60.Lj, 46.25.–y **DOI:** 10.1088/1674-1056/21/11/110207

1. Introduction

Meshless methods have attracted increasing attention in the scientific community in recent years. This is because in mesh-based techniques, such as the finite element method (FEM) and the boundary element method (BEM), the mesh generation for complex geometries is often arduous, time-consuming, and prone to errors. A major advantage of the meshless methods is that they do not require any element connectivity information and do not suffer much degradation in accuracy when the nodal arrangements are irregular. Up to now, there has been a wide variety of meshless methods [1] and they can usually be divided into two main categories: the boundary-type meshless method and the domain-type meshless method. Compared to the domain-type meshless method, the boundary-type one is undoubtedly superior, because it can provide accurate and complete solutions while reducing the dimensionality of any given problem by one, thus simplifying the effort involved in data preparation and reducing the computation time. Some representative boundary-type meshless methods include the boundary node method (BNM),[2,3] the hybrid boundary node method (HBNM),[4,5] the singular hybrid boundary node method (SHBNM),[6] the dual reciprocity hybrid boundary node method (DHBNM),[7,8] the boundary element-free method (BEFM),[9,10] and the moving Kriging interpolation-based boundary node method (MKIBNM).[11] Unfortunately, those methods involve the singular integration and hence are mathematically complicated due to the use of the fundamental solutions. As an improved boundary-type meshless method, the boundary knot method (BKM)[12,13] is based on a nonsingular general solution and hence mathematically simple and easy to implement. However, the introduction of the nonsingular kernels may jeopardize the accuracy of the solutions as comparing with those using the singular fundamental solutions.[14] Consequently, the efficiency and the accuracy of the boundary-type meshless method still need to be further improved.

Involving the discretization of the boundary only, the scaled boundary finite element method (SBFEM)

*Project supported by the National Natural Science Foundation of China (Grant No. 11002054).

†Corresponding author. E-mail: chenshenshen@tsinghua.org.cn

© 2012 Chinese Physical Society and IOP Publishing Ltd

developed recently by Wolf and Song[15] does not require any fundamental solution. This method uses a scaled coordinate system that scales the boundary to a single point called the scaling center. The weighted residual technique is applied in the circumferential direction, and then the governing partial differential equations are transformed into the scaled boundary equations in displacement, a system of linear second-order ordinary differential equations with the radial coordinate as the independent variable. The SBFEM is semi-analytical, as the ordinary differential equations can be solved analytically, which permits an efficient and highly accurate calculation of the stress intensity factors (SIFs).[16−19] Recently, the moving least squares (MLS) approximation has been combined with the scaled boundary equation to produce the meshless local Petrov–Galerkin scaled boundary method (MLPGSBM).[20] As a result, this method requires only a nodal data structure on the boundary and possesses a semi-analytical property along the radial direction. However, the shape functions based on the MLS approximation lack the δ function property, thus the accurate imposition of the essential boundary conditions requires additional techniques, which makes the MLPGSBM computationally much more expensive than the conventional SBFEM.

The moving Kriging (MK) interpolation was first employed to construct the meshless shape functions by Gu,[21] who successfully demonstrated the effectiveness of the MK formulation in solving the one-dimensional steady-state heat conduction. Soon after, this technique was extensively explored for possible applications in meshless methods.[22−25] A salient advantage of the MK interpolation is that the shape functions in this way satisfy the δ function property, thus the essential boundary conditions can be enforced easily without using any special techniques. In addition, since the MK interpolation is based on the statistical theories for minimum mean square error, it can ensure the interpolation accuracy and exactly reproduces any function included in its basis. Despite the fact that the MK interpolation has shown such a good potential, its application in the meshless methods is still in the very beginning stage.

In this paper, a boundary-type meshless method called the scaled boundary node method (SBNM) is developed and applied to two-dimensional crack problems. The MK interpolation based on the scattered nodes on the boundary is adopted to construct the shape functions in the circumferential direction. Due to the combination of the intrinsic analytical property along the radial direction and the higher continuity property of the MK interpolation, the stress intensity factors (SIFs) can be obtained directly and accurately by using a small number of freedoms and a small amount of computation time. Numerical examples analyzing two-dimensional crack problems are presented and discussed to demonstrate the applicability and the efficiency of the scaled boundary node method.

2. The moving Kriging interpolation

This section gives a brief summary of the moving Kriging interpolation, excellent illustrations can be found in Refs. [13] and [21]–[25].

Similar to the HBNM, the MK interpolation is independently performed on piecewise smooth edges S_i, $i = 1, 2, \ldots, M$, which constitute the boundary naturally, rather than on the whole boundary S. Let us assume that $u(s)$ is a random function, which is defined in a single edge discretized by N nodes at random locations s_1 to s_N, where s is the arc length denoting the distance around the edge from an origin on the edge. It is also assumed that only n nodes surrounding point s contribute to $u(s)$. The domain that includes these surrounding nodes is defined as the interpolation domain. Thus, the estimated value of function $u(s)$ at point s, $u^h(s)$, can be given as

$$u^{\mathrm{h}}(s) = \sum_{I=1}^{n} \phi_I(s) u_I = \boldsymbol{\Phi}(s)\boldsymbol{u}, \tag{1}$$

where $\boldsymbol{u} = \left[\, u(s_1),\ u(s_2),\ \ldots,\ u(s_n) \,\right]^{\mathrm{T}}$, and $\boldsymbol{\Phi}(s)$ is a $1 \times n$ vector of shape functions, expressed as

$$\boldsymbol{\Phi}(s) = \boldsymbol{p}^{\mathrm{T}}(s)\boldsymbol{A} + \boldsymbol{r}^{\mathrm{T}}(s)\boldsymbol{B}. \tag{2}$$

Matrices $\boldsymbol{A}$ and $\boldsymbol{B}$ are determined respectively by

$$\boldsymbol{A} = (\boldsymbol{P}^{\mathrm{T}}\boldsymbol{R}^{-1}\boldsymbol{P})^{-1}\boldsymbol{P}^{\mathrm{T}}\boldsymbol{R}^{-1}, \tag{3}$$

$$\boldsymbol{B} = \boldsymbol{R}^{-1}(\boldsymbol{I} - \boldsymbol{P}\boldsymbol{A}), \tag{4}$$

where $\boldsymbol{I}$ is a unit matrix of size $n \times n$, and $\boldsymbol{p}(s) = \left[\, p_1(s)\ p_2(s)\ \ldots\ p_m(s) \,\right]^{\mathrm{T}}$ is a complete monomial basis of order m. In the numerical implementation presented later in this paper, a linear basis is used, i.e.,

$$\boldsymbol{p}^{\mathrm{T}}(s) = \left(\, 1\ s \,\right), \quad m = 2. \tag{5}$$

The $n \times m$ matrix $\boldsymbol{P}$ that has the evaluated function values at the given set of nodes is defined as

$$\boldsymbol{P} = \begin{bmatrix} \boldsymbol{p}(s_1) \\ \vdots \\ \boldsymbol{p}(s_n) \end{bmatrix} = \begin{bmatrix} p_1(s_1) & p_2(s_1) & \dots & p_m(s_1) \\ p_1(s_2) & p_2(s_2) & \dots & p_m(s_2) \\ \vdots & \vdots & \ddots & \vdots \\ p_1(s_n) & p_2(s_n) & \dots & p_m(s_n) \end{bmatrix}. \quad (6)$$

Matrix $\boldsymbol{R}$ and vector $\boldsymbol{r}(s)$ are given by the following equations:

$$\boldsymbol{R}[R(s_i, s_j)] = \begin{bmatrix} 1 & R(s_1, s_2) & \dots & R(s_1, s_n) \\ R(s_2, s_1) & 1 & \dots & R(s_2, s_n) \\ \vdots & \vdots & \ddots & \vdots \\ R(s_n, s_1) & R(s_n, s_2) & \dots & 1 \end{bmatrix}, \quad (7)$$

$$\boldsymbol{r}^{\mathrm{T}}(s) = \begin{bmatrix} R(s, s_1) & R(s, s_2) & \dots & R(s, s_n) \end{bmatrix}, \quad (8)$$

where $R(s_i, s_j)$ is the correlation function between any pair of nodes located at s_i and s_j. There are various functions that can be selected. In this paper, the frequently and widely used Gaussian function is employed

$$R(s_i, s_j) = \exp(-\theta r_{ij}^2), \quad (9)$$

where $r_{ij} = \|s_i - s_j\|$, and $\theta > 0$ is a correlation parameter of the model. The shape function obtained from the MK interpolation possesses the following δ function property:

$$\phi_I(s_J) = \delta_{IJ} = \begin{cases} 1, & (I = J; I, J = 1, 2, \dots, n), \\ 0, & (I \neq J; I, J = 1, 2, \dots, n). \end{cases} \quad (10)$$

Another important property of the MK shape functions is that it can reproduce any function included in the basis exactly. In particular, if all constants and linear terms are included, it reproduces the general linear polynomial exactly, that is,

$$\sum_{I=1}^{n} \phi_I(s) = 1, \quad \sum_{I=1}^{n} \phi_I(s) s_I = s. \quad (11)$$

In order to define the interpolation domain for a point, a curvilinear interpolation domain is employed. The arc length of the curvilinear local interpolation domain d_{m} is computed by

$$d_{\mathrm{m}} = \alpha d_{\mathrm{c}}, \quad (12)$$

where d_{c} is the characteristic arc length relative to the nodal spacing close to the point of interest, while coefficient α stands for the scaling factor, and $\alpha = 4.0$ is employed in the present work. In addition, the correlation parameter θ in Eq. (9) can be obtained by[23]

$$\theta = \omega / h^2, \quad (13)$$

where ω is a constant and taken to be 0.1 here, and h is the average nodal spacing in the interpolation domain.

3. SBNM formulation

The linear elasticity problem is a classical boundary value problem (BVP) in mechanical analysis, which is governed by equilibrium equations, strain-displacement equations, constitutive equations, and two sets of boundary conditions. Generally, the analytical solutions for most problems cannot be obtained easily, numerical methods, such as FEM, BEM, and SBFEM, need to be employed to obtain the approximate solutions. The equations of elasticity can be written as

$$\boldsymbol{L}^{\mathrm{T}} \boldsymbol{\sigma} + \boldsymbol{f} = 0, \quad (14)$$

$$\boldsymbol{\varepsilon} = \boldsymbol{L} \boldsymbol{u}, \quad (15)$$

$$\boldsymbol{\sigma} = \boldsymbol{D} \boldsymbol{\varepsilon} = \boldsymbol{D} \boldsymbol{L} \boldsymbol{u}, \quad (16)$$

where $\boldsymbol{\sigma}$, $\boldsymbol{\varepsilon}$, and $\boldsymbol{f}$ are the stress vector, the strain vector, and the body load, respectively, $\boldsymbol{D}$ and $\boldsymbol{u}$ denote the elasticity matrix of the structure and the displacements, respectively, and $\boldsymbol{L}$ is the linear operator matrix and can be given explicitly as

$$\boldsymbol{L} = \begin{bmatrix} \partial/\partial x & 0 \\ 0 & \partial/\partial y \\ \partial/\partial y & \partial/\partial x \end{bmatrix}. \quad (17)$$

The corresponding boundary conditions are

$$\boldsymbol{u} = \bar{\boldsymbol{u}} \quad \text{on the essential boundary } S_u, \quad (18)$$

$$\boldsymbol{\sigma} \cdot \boldsymbol{n} = \bar{\boldsymbol{t}} \quad \text{on the natural boundary } S_t, \quad (19)$$

where $\bar{\boldsymbol{u}}$ and $\bar{\boldsymbol{t}}$ are the prescribed displacements and tractions, respectively , and $\boldsymbol{n}$ is the unit vector outward normal to boundary S ($S = S_u \cup S_t$).

The numerical method explored in this work to solve the above linear elasticity problem is the scaled boundary node method, in which the so-called scaled boundary coordinate system[15−20] is introduced. As shown in Fig. 1, this coordinate system scales the domain boundary S relative to a scaling center O, from

which the total boundary S must be visible. The circumferential coordinate s measures the distance anticlockwise around the boundary S. The radial coordinate ξ is defined to be zero at the scaling center, unit value at the boundary S, and infinity for far field. The formula of transformation from the Cartesian coordinate system to the scaled boundary coordinate system can be written as

$$\hat{x} = \hat{x}_0 + \xi x(s), \quad \hat{y} = \hat{y}_0 + \xi y(s), \tag{20}$$

where $(\hat{x}_0, \hat{y}_0)$ is the scaling center, $(x(s), y(s))$ is an arbitrary point on the boundary, and $(\hat{x}, \hat{y})$ is an interior point in the domain.

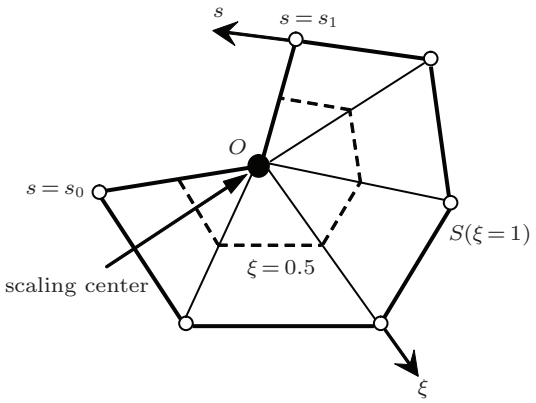


Fig. 1. Scaled boundary coordinate system.

Using the scaled boundary transformation detailed by Song and Wolf,[15] the linear operator matrix $\boldsymbol{L}$ in Eq. (17) can be written as

$$\boldsymbol{L} = \boldsymbol{b}^1(s)\frac{\partial}{\partial \xi} + \frac{1}{\xi}\boldsymbol{b}^2(s)\frac{\partial}{\partial s}, \tag{21}$$

where $\boldsymbol{b}^1(s)$ and $\boldsymbol{b}^2(s)$ depend only on the geometry of the boundary and can be expressed in the form

$$\boldsymbol{b}^1(s) = \frac{1}{|J|}\begin{bmatrix} y(s)_{,s} & 0 \\ 0 & -x(s)_{,s} \\ -x(s)_{,s} & y(s)_{,s} \end{bmatrix},$$
$$\boldsymbol{b}^2(s) = \frac{1}{|J|}\begin{bmatrix} -y(s) & 0 \\ 0 & x(s) \\ x(s) & -y(s) \end{bmatrix}, \tag{22}$$

with the Jacobian $|J|$ at the boundary ($\xi = 1$) being defined as

$$|J| = x(s)y(s)_{,s} - y(s)x(s)_{,s}. \tag{23}$$

Based on the meshless shape functions given in Eq. (2), the SBNM seeks an approximate solution in the form

$$\boldsymbol{u}(\xi, s) = \boldsymbol{\Phi}(s)\boldsymbol{u}(\xi), \tag{24}$$

where $\boldsymbol{u}(\xi)$ is the displacement function in the radial direction.

By substituting Eqs. (21) and (24) into Eq. (16), the stresses $\boldsymbol{\sigma}(\xi, s)$ can be obtained in the scaled boundary coordinate system as

$$\boldsymbol{\sigma}(\xi, s) = \boldsymbol{D}\left(\boldsymbol{B}^1(s)\boldsymbol{u}(\xi)_{,\xi} + \frac{1}{\xi}\boldsymbol{B}^2(s)\boldsymbol{u}(\xi)\right), \tag{25}$$

with two matrices $\boldsymbol{B}^1(s)$ and $\boldsymbol{B}^2(s)$ being formulated as

$$\boldsymbol{B}^1(s) = \boldsymbol{b}^1(s)\boldsymbol{\Phi}(s), \quad \boldsymbol{B}^2(s) = \boldsymbol{b}^2(s)\boldsymbol{\Phi}(s)_{,s}. \tag{26}$$

For the case without the body and the side face loads, the virtual work statement can be expressed as

$$\int_{\Omega} \delta\boldsymbol{\varepsilon}(\xi, s)^{\mathrm{T}}\boldsymbol{\sigma}(\xi, s)\mathrm{d}\Omega - \int_{S_t} \delta\boldsymbol{u}(s)^{\mathrm{T}}\bar{\boldsymbol{t}}(s)\mathrm{d}s = 0. \tag{27}$$

The Galerkin approach is taken, and the virtual displacement fields of the same form as Eq. (24) are employed. Through a series of manipulations detailed by Deeks and Wolf,[26] we find that equation (27) is satisfied for all virtual displacement fields when both the following conditions are simultaneously satisfied:

$$\boldsymbol{P} = \boldsymbol{E}^0\boldsymbol{u}(\xi)_{,\xi} + \boldsymbol{E}^{1\,\mathrm{T}}\boldsymbol{u}(\xi)\,|_{\xi=1}\,, \tag{28}$$
$$\boldsymbol{E}^0\xi^2\boldsymbol{u}(\xi)_{,\xi\xi} + \left(\boldsymbol{E}^0 + \boldsymbol{E}^{1\,\mathrm{T}} - \boldsymbol{E}^1\right)\xi\boldsymbol{u}(\xi)_{,\xi} - \boldsymbol{E}^2\boldsymbol{u}(\xi) = \boldsymbol{0}, \tag{29}$$

where

$$\boldsymbol{P} = \int_{S_t} \boldsymbol{\Phi}(s)^{\mathrm{T}}\bar{t}\mathrm{d}s, \tag{30}$$
$$\boldsymbol{E}^0 = \int_S \boldsymbol{B}^1(s)^{\mathrm{T}}\boldsymbol{D}\boldsymbol{B}^1(s)\,|J|\,\mathrm{d}s, \tag{31}$$
$$\boldsymbol{E}^1 = \int_S \boldsymbol{B}^2(s)^{\mathrm{T}}\boldsymbol{D}\boldsymbol{B}^1(s)\,|J|\,\mathrm{d}s, \tag{32}$$
$$\boldsymbol{E}^2 = \int_S \boldsymbol{B}^2(s)^{\mathrm{T}}\boldsymbol{D}\boldsymbol{B}^2(s)\,|J|\,\mathrm{d}s, \tag{33}$$

Equation (29) is the so-called scaled boundary equation in displacement. The governing equations have been effectively weakened in the circumferential direction, but remain strong in the radial direction. Clearly, the spatial dimension in the SBNM is reduced by one as the case in the boundary element method.

At the expense of doubling the number of degrees of freedom, the homogeneous second-order differential equations in Eq. (29) can be transformed into the first-order ordinary differential equations

$$\xi \boldsymbol{X}(\xi)_{,\xi} = -\boldsymbol{Z}\boldsymbol{X}(\xi) \tag{34}$$

by introducing variable $\boldsymbol{X}(\xi)$ and Hamiltonian matrix $\boldsymbol{Z}$

$$\boldsymbol{X}(\xi) = \begin{Bmatrix} \boldsymbol{u}(\xi) \\ \boldsymbol{q}(\xi) \end{Bmatrix},$$
$$\boldsymbol{Z} = \begin{bmatrix} \boldsymbol{E}^{0^{-1}}\boldsymbol{E}^{1^{\mathrm{T}}} & -\boldsymbol{E}^{0^{-1}} \\ \boldsymbol{E}^{1}\boldsymbol{E}^{0^{-1}}\boldsymbol{E}^{1^{\mathrm{T}}} - \boldsymbol{E}^{2} & -\boldsymbol{E}^{1}\boldsymbol{E}^{0^{-1}} \end{bmatrix}, \tag{35}$$

where $\boldsymbol{q}(\xi)$ is the internal nodal forces on a surface with a constant ξ and is expressed as

$$\boldsymbol{q}(\xi) = \boldsymbol{E}^{0}\xi\boldsymbol{u}(\xi)_{,\xi} + \boldsymbol{E}^{1^{\mathrm{T}}}\boldsymbol{u}(\xi). \tag{36}$$

In the eigenvalue method,[16] the following eigenvalue problem has to be solved:

$$\boldsymbol{Z}\begin{bmatrix} \boldsymbol{\Phi}_{11} & \boldsymbol{\Phi}_{12} \\ \boldsymbol{\Phi}_{21} & \boldsymbol{\Phi}_{22} \end{bmatrix} = \begin{bmatrix} \boldsymbol{\Phi}_{11} & \boldsymbol{\Phi}_{12} \\ \boldsymbol{\Phi}_{21} & \boldsymbol{\Phi}_{22} \end{bmatrix}\begin{bmatrix} \boldsymbol{\Lambda}_0 & \\ & -\boldsymbol{\Lambda}_0 \end{bmatrix},$$
$$\boldsymbol{\Lambda}_0 = [\lambda_i]\,. \tag{37}$$

The real parts of all elements λ_i are non-positive. The general solutions of $\boldsymbol{u}(\xi)$ and $\boldsymbol{q}(\xi)$ can be expressed as

$$\boldsymbol{u}(\xi) = \boldsymbol{\Phi}_{11}\xi^{-\boldsymbol{\Lambda}_0}\boldsymbol{c}_1 + \boldsymbol{\Phi}_{12}\xi^{\boldsymbol{\Lambda}_0}\boldsymbol{c}_2, \tag{38}$$
$$\boldsymbol{q}(\xi) = \boldsymbol{\Phi}_{21}\xi^{-\boldsymbol{\Lambda}_0}\boldsymbol{c}_1 + \boldsymbol{\Phi}_{22}\xi^{\boldsymbol{\Lambda}_0}\boldsymbol{c}_2. \tag{39}$$

For a bounded medium, the displacements at $\xi = 0$ must remain finite. Since the real parts of λ_i in $\boldsymbol{\Lambda}_0$ are non-positive, Eqs. (38) and (39) are reduced to

$$\boldsymbol{u}(\xi) = \boldsymbol{\Phi}_{11}\xi^{-\boldsymbol{\Lambda}_0}\boldsymbol{c}_1, \tag{40}$$
$$\boldsymbol{q}(\xi) = \boldsymbol{\Phi}_{21}\xi^{-\boldsymbol{\Lambda}_0}\boldsymbol{c}_1. \tag{41}$$

The stiffness matrix $\boldsymbol{K}^{\mathrm{b}}$ for the bounded medium with respect to the boundary degrees of freedom is therefore

$$\boldsymbol{K}^{\mathrm{b}} = \boldsymbol{\Phi}_{21}\boldsymbol{\Phi}_{11}^{-1}, \tag{42}$$

and the equilibrium requirement is reduced to

$$\boldsymbol{K}^{\mathrm{b}}\boldsymbol{u} = \boldsymbol{P}, \tag{43}$$

where $\boldsymbol{P}$ is the nodal force vector defined in Eq. (30), and $\boldsymbol{u}$ is the boundary node displacement vector. It is worthwhile noting that because the shape functions constructed by the MK interpolation possess the δ function property, the essential boundary conditions can be implemented straightforwardly. After solving for $\boldsymbol{u}$, the integration constant $\boldsymbol{c}_1$ can be obtained as

$$\boldsymbol{c}_1 = \boldsymbol{\Phi}_{11}^{-1}\boldsymbol{u}. \tag{44}$$

After $\boldsymbol{c}_1$ is determined, the substitution of Eq. (40) into Eqs. (24) and (25) then provides the entire displacement and stress fields.

4. Numerical examples

In this section, the proposed SBNM formulation is applied to stress intensity factor analyses of two-dimensional crack problems. These examples are employed to verify the performance of the numerical technique. In all calculations, the scaling center is placed at the crack tip, and the stress intensity factors of mode I and mode II are directly evaluated based on their definitions

$$K_{\mathrm{I}} = \lim_{\hat{r}\to 0}\sqrt{2\pi\hat{r}}\sigma_{yy}\,|_{\theta=0}\,, \tag{45a}$$
$$K_{\mathrm{II}} = \lim_{\hat{r}\to 0}\sqrt{2\pi\hat{r}}\sigma_{xy}\,|_{\theta=0}\,, \tag{45b}$$

where the crack is assumed to lie on the negative $\hat{x}$ axis, and $\hat{r}$ and θ are the polar coordinates with the origin at the crack tip, as shown in Fig. 2.

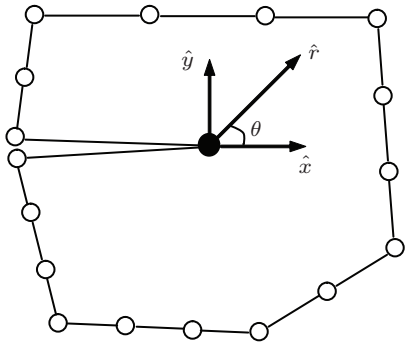


Fig. 2. cracked domain modeled by the SBNM.

4.1. Square plate with an edge crack

The first example corresponds to an edge crack in a square plate loaded with uniform tensile stress σ, as shown in Fig. 3. The straight crack of length a is perpendicular to the side of length b. A total of 33 boundary nodes (Fig. 3) are used to discretize the boundary of the problem. It should be noted that at point A where the crack intersects the boundary, two independent nodes with the same coordinates are

placed. The mode I SIFs normalized with $\sigma\sqrt{\pi a}$ are listed for various crack lengths ($a/b = 0.2$ to 0.6) in Table 1. The analytical solutions from Ref. [27] are also shown in Table 1. It is observed that the mode I SIFs obtained by the present SBNM are in excellent agreement with the analytical solutions. Note that the numbers of nodes employed in the computation is rather small.

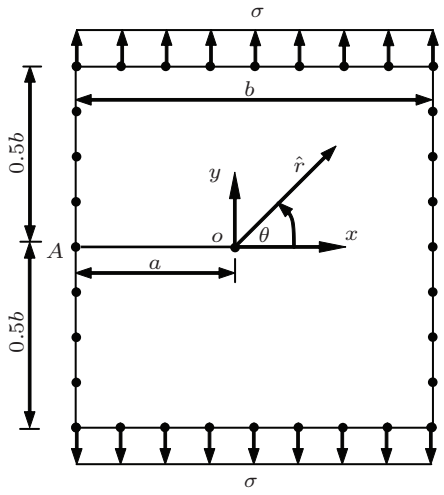


Fig. 3. A square plate with an edge crack.

Table 1. Normalized mode I SIFs ($K_{\rm I}/\sigma\sqrt{\pi a}$) for various crack lengths a/b.

a/b	Present	Analytical solution[27]
0.2	1.488	1.488
0.3	1.848	1.848
0.4	2.324	2.325
0.5	3.009	3.010
0.6	4.149	4.153

4.2. Rectangular plate with an inclined central crack

An inclined central crack of length $2a$ in a rectangular plate of height $2h$ and width $2w$ with an inclination angle of θ is considered here, as shown in Fig. 4. The mixed-mode loading is achieved by a uniform tensile stress σ applied to the ends of the plate. The ratio between the height and the width of the plate is chosen to be 2.0, i.e., $h/w = 2.0$. The problem has also been numerically investigated using the conformal mapping (CMAP) approach[28] and the super singular element method.[29]

As shown in Fig. 5, the plate is divided into two subdomains, and their scaling centers are chosen at the two crack tips. The boundary of each subdomain is discretized with 71 boundary nodes. It should be noted that there are two overlapping nodes, one for each crack face, at the center of the plate. Table 2 presents the mixed mode SIFs $K_{\rm I}$ and $K_{\rm II}$ for various crack lengths and angles of inclination. This table also shows the results given in Refs. [28] and [29]. Again, the agreement appears to be very good. This further demonstrates that the present numerical method can be applied for the mixed mode fracture analysis more easily with relatively few degrees of freedom than the other computational methods.

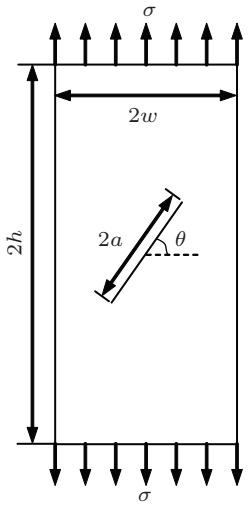


Fig. 4. A rectangular plate with an inclined central crack.

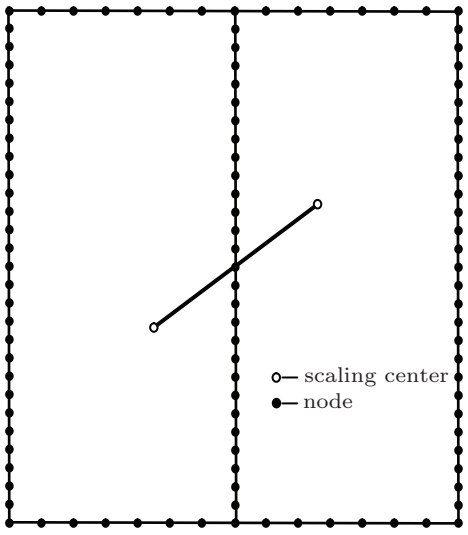


Fig. 5. SBNM mesh of the plate with an inclined central crack.

Table 2. Normalized mixed mode SIFs for various lengths of inclined central crack at 15°, 30°, and 45°.

a/w	$K_{\rm I}/\sigma\sqrt{\pi a}$			$K_{\rm II}/\sigma\sqrt{\pi a}$		
	CMAP[28]	SSEM[29]	Present	CMAP[28]	SSEM[29]	Present
$\theta = 15°$						
0.3	0.9904	0.9901	0.9908	0.2527	0.2528	0.2538
0.4	1.0402	1.0400	1.0401	0.2560	0.2561	0.2565
0.5	1.1128	1.1126	1.1122	0.2619	0.2620	0.2624
0.6	1.2183	1.2183	1.2165	0.2725	0.2727	0.2730
0.7	1.378	1.3778	1.3723	0.290	0.2930	0.2898
$\theta = 30°$						
0.3	0.8025	0.8024	0.8037	0.4417	0.4417	0.4424
0.4	0.8456	0.8455	0.8464	0.4497	0.4497	0.4496
0.5	0.9046	0.9048	0.9053	0.4617	0.4617	0.4616
0.6	0.984	0.9838	0.9843	0.480	0.4802	0.4800
0.7	1.091	1.0864	1.0907	0.508	0.5102	0.5079
$\theta = 45°$						
0.3	0.5406	0.5405	0.5406	0.5162	0.5161	0.5197
0.4	0.5719	0.5719	0.5721	0.5290	0.5288	0.5295
0.5	0.6119	0.6121	0.6122	0.5458	0.5457	0.5461
0.6	0.6611	0.6605	0.6619	0.5674	0.5676	0.5674
0.7	0.721	0.7154	0.7224	0.595	0.5953	0.5945

5. Conclusion

A new formulation of the boundary-type meshless method, called the scaled boundary node method, is presented for two-dimensional fracture analysis in this paper. In comparison with the traditional SBFEM, this method is a meshless method, because the moving Kriging interpolation is introduced, and thus no element connectivity is required in constructing the shape function in the circumferential direction. Furthermore, the shape function constructed using the moving Kriging interpolation possesses the δ function property, therefore no special treatment is needed to impose the essential boundary conditions. As demonstrated by the computational results, the present approach can be applied to solve two-dimensional crack problems efficiently and accurately due to the analytical property in the radial direction. No post-processing is needed to extract the stress intensity factors. Further research for developing the SBNM to model three-dimensional crack problems is in progress.

Acknowledgement

The authors wish to thank Dr. Song Chong-Min from the University of New South Wales for his valuable assistance.

References

[1] Zhang X, Liu Y and Ma S 2009 *Advances in Mechanics* **39** 1 (in Chinese)

[2] Mukherjee Y X and Mukherjee S 1997 *Int. J. Numer. Meth. Eng.* **40** 797

[3] Kothnur V S, Mukherjee S and Mukherjee Y X 1999 *Int. J. Solids Struc.* **36** 1129

[4] Zhang J M, Yao Z H and Li H 2002 *Int. J. Numer. Meth. Eng.* **53** 751

[5] Zhang J M, Tanaka M and Matsumoto T 2004 *Int. J. Numer. Meth. Eng.* **59** 1147

[6] Miao Y, Wang Y H and Yu F 2005 *Eng. Anal. Bound. Elem.* **29** 703

[7] Yan F, Wang Y H, Miao Y and Tan F 2008 *Acta Mech. Solida Sin.* **21** 267

[8] Yan F, Wang Y H, Miao Y, Tham L G and Cheung Y K 2009 *J. Sound Vib.* **321** 1036

[9] Peng M J and Cheng Y M 2009 *Eng. Anal. Bound. Elem.* **33** 77

[10] Liew K M, Cheng Y M and Kitipornchai S 2007 *Int. J. Solids Struct.* **44** 4220

[11] Li X G, Dai B D and Wang L H 2010 *Chin. Phys.* B **19** 120202

[12] Chen W, Shen L J, Shen Z J and Yuan G W 2005 *Eng. Anal. Bound. Elem.* **29** 756

[13] Hon Y C and Chen W 2003 *Int. J. Numer. Meth. Eng.* **56** 1931

[14] Young D L, Chen K H and Lee C W 2005 *J. Comput. Phys.* **209** 290
[15] Song C and Wolf J 1997 *Comput. Methods Appl. Mech. Eng.* **147** 329
[16] Song C and Wolf J 2002 *Comput. Struct.* **80** 183
[17] Song C 2006 *Int. J. Numer. Meth. Eng.* **65** 620
[18] Liu J Y and Lin G 2007 *China Ocean Eng.* **21** 293
[19] Song C, Tin-Loi F and Gao W 2010 *Eng. Fract. Mech.* **77** 2316
[20] Deeks A J and Augarde C E 2005 *Comput. Mech.* **36** 159
[21] Gu L 2003 *Int. J. Numer. Meth. Eng.* **56** 1
[22] Zheng B J and Dai B D 2010 *Acta Phys. Sin.* **59** 5182 (in Chinese)
[23] Zheng B J and Dai B D 2011 *Appl. Math. Comput.* **218** 563
[24] Zhu P and Liew K M 2011 *Compos. Struct.* **93** 2925
[25] Bui Q T, Nguyen N M, Zhang Ch and Pham DAK 2011 *Smart Mater. Struct.* **20** 1
[26] Deeks A J and Wolf J P 2002 *Comput. Mech.* **28** 489
[27] Civelek M B and Erdogan F 1982 *Int. J. Fract.* **19** 139
[28] Kitagawa H and Yuuki R 1977 *Trans. Jpn. Soc. Mech. Eng.* **43** 4354
[29] Tsang D K L and Oyadiji S O 2008 *Proc. R. Soc.* A **464** 2629